Journal of Structural Geology 31 (2009) 1295–1307

Contents lists available at ScienceDirect

Journal of Structural Geology

journal homepage: www.elsevier.com/locate/jsg

The mechanism of flow and fabric development in mechanically anisotropic trachyte lava

Prokop Závada [a,*], Karel Schulmann [b], Ondrej Lexa [c], František Hrouda [d], Jakub Haloda [e], Patricie Týcová [e]

[a] Department of Tectonics and Geodynamics, Institute of Geophysics AS CR, v.v.i., Boční II/1401, 141 31 Prague 4, Czech Republic
[b] Centre de Géochimie de la Surface, EOST, Université Louis Pasteur, Strasbourg Cedex, France
[c] Institute of Petrology and Structural Geology, Charles University, Prague, Czech Republic
[d] Agico Inc., Brno, Czech Republic
[e] Czech Geological Survey, Klárov 3, Prague, Czech Republic

ARTICLE INFO

Article history:
Received 18 August 2008
Received in revised form
23 March 2009
Accepted 12 April 2009
Available online 18 April 2009

Keywords:
Trachyte
Lava dome
Fibre-slip mechanism
Mechanical anisotropy
Sanidine
Anisotropy of magnetic susceptibility

ABSTRACT

Anisotropy of magnetic susceptibility (AMS) and Electron back-scattered diffraction (EBSD) of magnetite and sanidine fabrics throughout an eroded trachyte lava dome in Tertiary volcanic province of the NW Czech Republic revealed two fabric types. The high degree of AMS fabric is associated with sanidine textural domains similar to normal kink bands (Type I fabric) and occupies the whole body except the SW margin. Folded fabric and low anisotropy of AMS also in the SW margin reveals sanidine alignment domains resembling reverse kink-bands (Type II fabric). The flow of trachyte lava occurred via simultaneous slip of sanidine crystals along their (010) planes and also by readjustment of the textural domain boundaries according to the fibre-slip theory. This microfabric study suggests that the Type II fabrics resulted from collapse of vertically anisotropic trachyte crystal mush above the feeding conduit. Type I fabric is interpreted to originate from Type II fabrics by further stretching of highly attenuated fold limbs. Asymmetric Type I fabrics along margins of the dome are related to outflow of trachyte lava away from the conduit region due to divergent flow. The trachyte fabric zonality is interpreted to reflect the process of successive emplacement of progressively rotated trachyte lava lobes within a lava dome that locally preserves the collapsed and folded vertical fabrics.

1. Introduction

The investigation of fabrics generated by lava flows requires structural, microstructural and quantitative fabric analyses (Smith, 2002). However, the small size of fabric elements makes microstructural studies difficult, so that analysis of anisotropy of magnetic susceptibility (AMS) is often employed (for review see Tarling and Hrouda, 1993).

Studies regarding fabrics in lavas focused mainly on basalts forming dykes or lava flows (Kolofíková, 1976; Raposo and Ernesto, 1995; Herrero-Bervera et al., 2001), or small aspect-ratio (height to width) rhyolitic domes (Fink, 1983; Smith and Houston, 1995; Merle, 1998; Buisson and Merle, 2002, 2004; Castro et al., 2002; Cañón Tapia and Castro, 2004; Maeno and Taniguchi, 2006). In contrast, systematic investigations of flow fabrics in crystal-rich volcanic extrusions that form large aspect-ratio domes or laccoliths are less common. Growth of these domes is typically by successive emplacement of "lobes" or "spines" of lava, which emerge and are transported sideways by newer lava lobes (Nakada et al., 1995; Melnik and Sparks, 1999; Sparks et al., 2000).

The internal fabric patterns of solidified phonolite or trachyte cupola-like bodies, which show high crystal content, were previously examined by the methods of structural analysis of macroscopic fluidality and jointing, X-ray diffraction and universal-stage (Cloos and Cloos, 1927; Varet, 1971; Jančušková et al., 1992). Introduction of the AMS technique allowed even more complex microstructural investigation of these cupolas (Arbaret et al., 1993). Utilisation of electron back-scattered diffraction (EBSD) and quantitative image analysis methods together with AMS can overcome the issues related to small grain size of fabric elements. The deformation/flow mechanism deciphered from trachyte fabrics using these methods is the focus of this paper.

In this study, a partly exposed trachyte body in the České středohoří Mountains is examined to determine the mechanisms of

* Corresponding author. Tel.: +420 267 103 074; fax: +420 272 761 549.
E-mail address: zavada@ig.cas.cz (P. Závada).

0191-8141/$ – see front matter © 2009 Elsevier Ltd. All rights reserved.
doi:10.1016/j.jsg.2009.04.002

lava flow and emplacement style. To quantify the rock fabrics related to flow and emplacement, we combine the AMS, EBSD and image analysis for the crystal preferred orientation (CPO) of tiny sanidine crystals. The spatial distribution and orientation of the fabrics is explained by a simple analogue model using plaster of Paris (Závada et al., 2008).

2. Geological setting

The Tertiary volcanic activity in the region of České středohoří Mountains is connected to the SW–NE trending continental Ohře (Eger) Rift (Špičák and Horálek, 2001; Uličný, 2001; Plomerová et al., 2003; Hrubcová et al., 2005) and can be divided into three main periods (Cajz et al., 1999): (1) weakly crustally-contaminated basanitic lavas with lherzolite xenoliths and volcanoclastics of 36–26 Ma age; (2) trachybasaltic lavas and volcaniclastics including trachytes and phonolites of bimodal tephrite/basanite–phonolite suite, marked by the lack of lherzolite xenoliths, and a 31–25 Ma age; and (3) flows of basanites, geochemically similar to the first group, about 24 Ma age. The first volcanic products form subvertical dykes or flows of lava along the major faults bounding the rift. The second-phase magmas intrude Cretaceous sedimentary rocks and the volcano-sedimentary sequences of the first phase along minor faults within the complex graben structure. These magmas were emplaced as shallow intrusive laccoliths, extrusive domes or intrusions into maar-diatremes (Kopecký, 1978; Ulrych et al., 2000).

From this second phase, a trachyte body Hradiště u Habří is investigated and is located 7 km E of Teplice town in North Bohemia (Fig. 1). The trachyte outcrop is elliptical, elongated in the NW direction in the plan-view, with a longer axis of 700 m. The vertical stratigraphical sequence in this area is documented from a deep drill hole GU 103 located ca. 1 km ENE from Hradiště hill (see inset in Fig. 1). The volcanic body, contains a sodalite-bearing trachyte to sodalite phonolite and is composed of approximately 78 vol.% of alkali feldspars (high sanidine), 12 vol.% foid minerals (sodalite to hauyne), 2 vol.% plagioclase and 5 vol.% aegirine–augite with magnetite, apatite and sphene as minor phases. In this study, we will call this rock a "trachyte" for simplicity, following Hrouda et al. (2005).

3. Structural and fabric data

3.1. Macroscopic structural pattern

The body forms a dome-like cupola, which is defined by regular set of planar fractures sub-parallel to a foliation defined by the alignment of sanidine phenocrysts up to 1 cm. These fractures are up to 1 m long, exhibit relatively high rugosity and their spacing ranges from 1 to 20 cm. They are macroscopically similar to "Flat-lying joints" from high structural levels of plutons (Cloos, 1922) and are designated as "F-joints" in this study (Fig. 2). Both "F-joints" and foliation defined by sanidine alignment dip steeply on the E, W and S rims of the body, show moderate dips on the slopes and are sub-horizontal in central part of the cupola.

A second joint set are steep joints radiating from the cupola centre (Figs. 2, 3) and are "Cross joints" of Cloos (1922). These fractures are generally smooth although some have plumose ornaments that range in length from 25 cm up to 3 m. Their spacing is between 2 and 3 m in the central part of cupola, 0.5–1 m on the western margin and locally only 5 cm (Fig. 3a) in the SW part of the body.

In the SW part of the trachytic cupola, the fabric defined by alignment of sanidine phenocrysts is refolded by open to close chevron folds with amplitudes up to 1 m (Fig. 3b). Fold axes are steep and axial planes dip steeply to the SW (Fig. 3a). Locally, the fabric shows irregular sinusoidal folding. Importantly, the "F-joints" are subparallel to the axial planes of the folds.

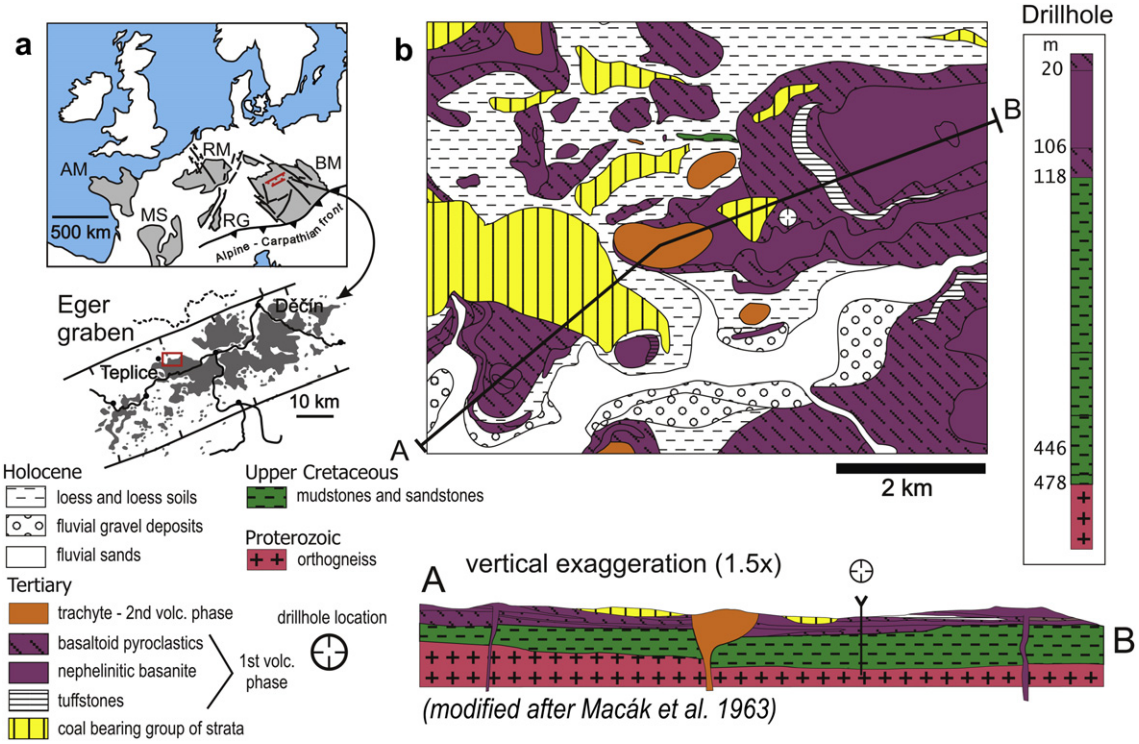

Fig. 1. (a) Position of the Eger rift in the European Variscides (grey) with deep seated faults active in the Tertiary shown and the extent of the České středohoří volcanic centre (grey in graben map) in the Eger graben (RG, Rhein graben; RM, Rhenish Massif; BM, Bohemian Massif; AM, Armorican Massif; MS, Massif Central). (b) Map and profile of study area and drill-hole lithological column (after Macák, 1963). The shape of the trachyte body in profile is hypothetical. Volcanic products of the third volcanic phase are not present in map area.

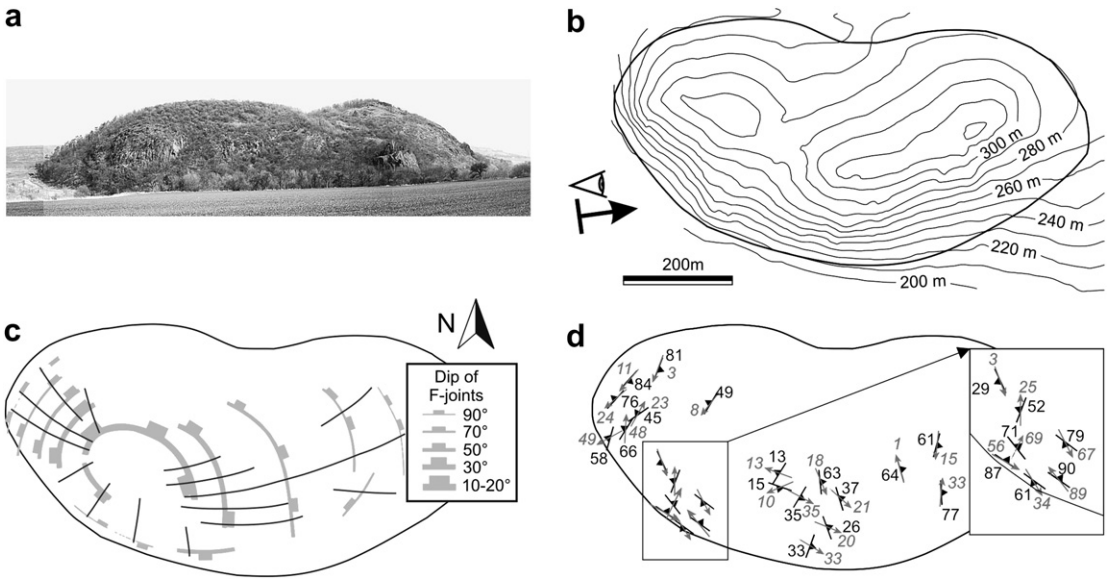

Fig. 2. (a) Photograph of the studied trachyte body showing outcrops on SW edge. (b) Topographical map of body (arrow indicates view for photograph in a). (c) Map of strike trends of "Flat lying joints" (F-joints) and "Cross joints". "F-joints" are grey contours with dip marks. Vertical "Cross joints" are black lines. (d) Map of dip directions and angles (black numbers) of magnetic foliation and plunge directions, and plunge angles (grey numbers) of magnetic lineation.

3.2. Microstructural data acquisition

3.2.1. AMS analysis

Oriented block samples were collected from trachyte outcrops and cubic specimens (2 cm wide) were cut for AMS measurement. AMS was measured with the KLY-4S Kappabridge (Jelínek et al., 1997; Pokorný et al., 2004) and the AMS data were statistically evaluated using the ANISOFT software (Jelínek, 1978; Hrouda et al., 1990). The degree of anisotropy (P), shape (T) and mean bulk susceptibility (K_m) of the AMS ellipsoid are characterised by the following parameters (Nagata, 1961; Jelínek, 1981):

$$P = K_1/K_3$$
$$T = (2\eta_2 - \eta_1 - \eta_3)/(\eta_1 - \eta_3)$$
$$K_m = (K_1 + K_2 + K_3)/3$$

where $K_1 > K_2 > K_3$ are the principal susceptibilities, $\eta_1 = \ln K_1$, $\eta_2 = \ln K_2$, $\eta_3 = \ln K_3$. The parameter P indicates the intensity of the preferred orientation of magnetic minerals in the rock. If $0 < T < +1$ the AMS ellipsoid is oblate (the magnetic fabric is planar); $T = +1$ means that the AMS ellipsoid is rotationally symmetric (uniaxial oblate). If $-1 < T < 0$ the AMS ellipsoid is prolate (the magnetic fabric is linear); $T = -1$ means that the AMS

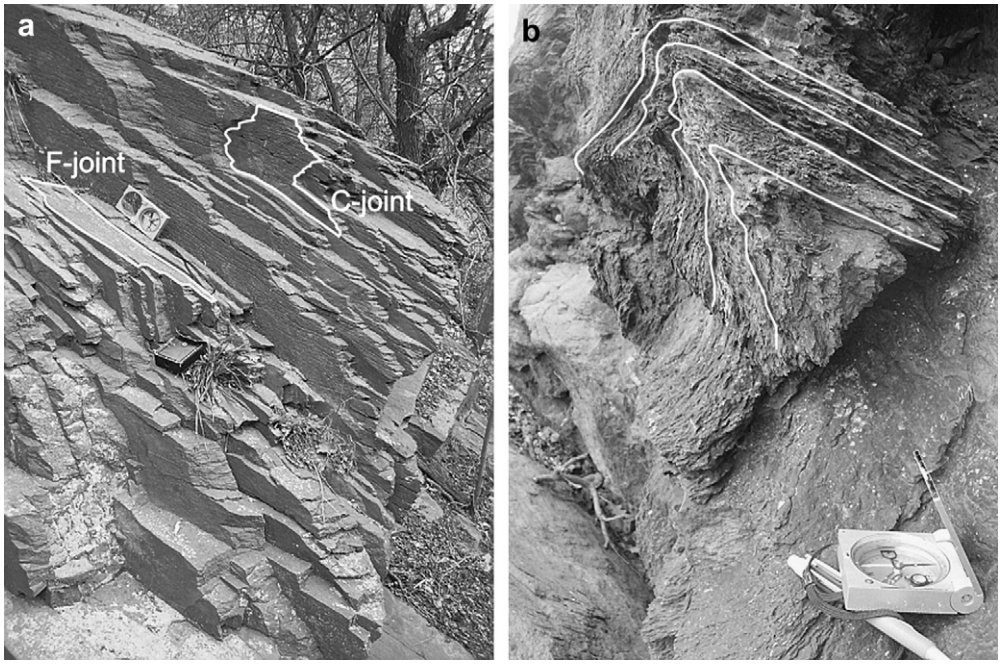

Fig. 3. Field photographs of trachyte outcrops. (a) Closely spaced subvertical "C-joints" and "F-joints" dipping at moderate angles, SW part of the body. (b) An asymmetric chevron fold with straight right limb and minor folds in the left limb. This outcrop collapsed due to erosion of the trachyte body. SW part of the body.

ellipsoid is uniaxial prolate. If $T = 0$ the ellipsoid is neither oblate nor prolate.

3.2.2. Fabric sample preparation

From each sample, two perpendicular thin-sections were cut parallel with K_1K_3 and K_2K_3 planes of the AMS ellipsoid for detailed microstructural analysis. For some samples, thin-sections parallel with K_1K_2 planes were also prepared. On the basis of AMS mean susceptibility directions and AMS parameter value variations (from 8 cubic specimens per sample) together with microscopic observations from the oriented thin-sections, two major fabric types were identified (Type I, Type II). Further AMS, and image and CPO analyses were performed to distinguish these two fabrics.

3.2.3. Image analysis

The two fabric types have different attitude of textural domains that are composed of groundmass sanidine laths and occur primarily in the vicinity of large phenocrysts. To quantify the relative abundance of these textural domains, both K_1K_3 and K_2K_3 thin-sections were photomicrographed using crossed polarised light and a gypsum plate for image analysis. For samples with conjugate sets of textural domains, two sets of micrographs per thin-section were taken and each domain was analysed separately, as each domain "lights up" at different angles, while rotating the microscope stage. Image colours were categorised using the public domain NIH Image program (developed at the U.S. National Institutes of Health, http://rsb.info.nih.gov/nih-image/). The colour range was divided into four: (1) textural domain, (2) surrounding groundmass, (3) transitional domains and (4) unclassified dark colours representing sodalite or augite phenocrysts, scratches, glue bubbles or voids.

3.2.4. CPO of groundmass sanidine

The crystallographic preferred orientation (CPO) of sanidine crystals was measured on a scanning electron microscope CamScan3200 (Czech Geological Survey, Prague). The acquired EBSD patterns were recorded using an HKL Technology NordlysII camera system and indexed using the Channel5 software of HKL Technology (Schmidt and Olensen, 1989) applying high sanidine crystallographic model of Scambos et al. (1987). Orientation contrast images were collected from forescatter detector (FSD) that is integrated into the NordlysII camera. Pattern acquisition was carried out at 20 kV acceleration voltage, ~5 nA beam current, 33 mm working distance and 70° sample tilt. Each thin-section was calibrated using a silicone monocrystal and only measurements with angular deviation below 1 were accepted. CPO measurement of sanidines from textural domains from 11 samples was carried out in manual mode. In this mode, position of electron beam on the sample and interpretation of the EBSD patterns are chosen by the operator. For Type I fabric samples, thin-sections parallel to K_1K_3 and K_2K_3 planes of the AMS ellipsoids were analysed. For Type II fabric, analysis of sections parallel to K_2K_3 was sufficient to describe the CPO, because this fabric is formed only by two sets of non-conjugate textural domains. All CPO datasets are rotated into geographical coordinates and plotted in stereographic projections.

3.3. Results

3.3.1. AMS fabric

The main carrier of magnetic susceptibility is magnetite with approximately 10% ilmenite content. The bulk susceptibility in the Hradiště trachyte is very high at about of 10^{-2} [SI] (Hrouda et al., 2005). The magnetic foliation throughout the Hradiště cupola conforms in azimuth and dip to the "F-joints" (Fig. 2d). The magnetic lineation shows shallow plunges in E and W marginal parts and trends parallel with the margin of the body. In the central part, lineation directions are subhorizontal too, but lack a consistent trend. In the SE part of the body, which reveals folded fabrics, lineation plunges at high angles (see inset of Fig. 2d). Contour diagrams of P and T parameters show lower values in the SE (folded) part of the body with respect to the rest of the cupola. The minimum P value in this area is 1.15, and for T is <0.2, while in the apical part and on the E and W margin of the cupola, P values range around 1.3 and T parameter values vary between 0.7 and 1 (Fig. 4).

3.3.2. Microstructural analysis from oriented thin-sections

The fabric of the trachyte has several microstructural elements: (1) alignment of large phenocrysts (sanidine and aegirine-augite), (2) textural domains defined by strong parallel alignment of sanidine microcrystals, (3) alignment of groundmass sanidine crystals not belonging to textural domains, and (4) AMS fabric derived from preferred orientation of titanomagnetite grains. Mean grain size is 10 μm for magnetic grains (obtained from image analysis of BSE images and statistically analysed using PolyLX Matlab toolbox (Lexa et al. (2005), http://petrol.natur.cuni.cz/~ondro/polylx:home) and 50–100 μm microsanidines. Magnetic grains have angular irregular shapes, average axial ratio 1.75 in K_1K_3 plane and eigenvalue ratio of the mean matrix of inertia 1.19 (Harvey and Ferguson, 1981). Preferred orientation of magnetite grain long axes is marked by two submaxima distributed at ca. 8° from the K_1 direction. The "Nearest Neighbor Index" R (Clark and Evans, 1954) revealed values 0.82, which suggests that the magnetite grains are slightly clustered (distribution is regular, random and clustered for $R > 1$, $R = 1$ and $R < 1$, respectively).

In Type I fabrics, textural domains occur in the groundmass as conjugate sets and are called conjugate textural domains (CTDs) (Fig. 5). These domains are similar to normal kink bands around boudins (Kidan and Cosgrove, 1996). In contrast, in Type II fabric, textural domains formed by tabular sanidine microcrystals resemble asymmetric reverse kink bands (Dewey, 1965). This fabric

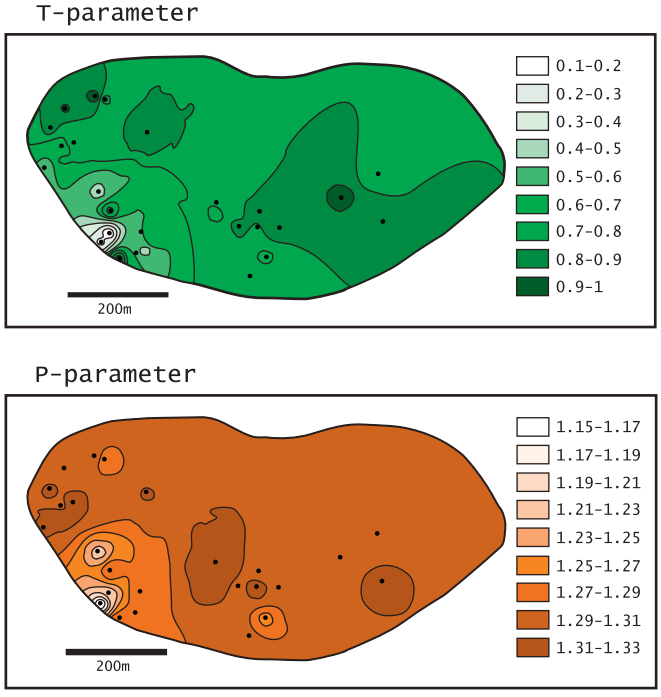

Fig. 4. Contoured diagram of the shape of the magnetic ellipsoid parameter T (a) and the degree of magnetic anisotropy parameter P (b) measured on 25 localities throughout the cupola.

is formed by two non-conjugate textural domains with variable abundance (Fig. 6).

3.3.3. Type I fabric

Type I fabric (Fig. 5) shows alignment of sanidine and aegirine–augite phenocrysts subparallel to the "F-joints". These phenocrysts have maximum 1 cm in their long dimension and comprise approximately 8 vol.% of the area in the thin-section. Most groundmass sanidine crystals show alignment subparallel with large phenocrysts. Conjugate textural domains (CTDs) emanate from corners of the phenocrysts at an angle ranging from 30° to 40° (from the phenocryst alignment trend in both K_1K_3, K_2K_3 thin-sections) and disappear at a distance of approximately half-length of the longer dimension of the specific phenocryst. The sanidine crystals in CTDs are aligned sub-parallel to domain boundaries. In samples, where the CTDs are equally developed, the K_3 mean susceptibility direction bisects the obtuse angles between the CTDs, while K_1 and K_2 directions bisect the acute angles. K_3 direction is also perpendicular to the alignment trend of large phenocrysts. In the K_1K_2 section, distinct zones of crystal alignment again oblique to magnetic lineation direction are also apparent around the larger phenocrysts and can be again regarded as CTDs (Fig. 5). The samples showing Type I fabrics are characterised by strongly oblate AMS ellipsoids ($T = 0.7$–0.9) and a large degree of anisotropy ($P = 1.29$–1.33). Type I fabrics occupy the whole cupola, except its SW part (Fig. 4, Table 1).

Most analysed Type I samples clearly display monoclinic fabric symmetry, as the textural domains are unequally represented in one of the perpendicular thin-sections (samples 18, 20, 23, 83; Table 1). Other samples show relatively balanced areal representation in both perpendicular thin-sections and can be regarded as orthorhombic (samples 38, 40).

Type I fabric is typical with narrow circular clusters of K_3 mean susceptibility direction of the AMS ellipsoid and clusters of K_1 and K_2 directions extending along the magnetic foliation plane up to girdle-like distribution for samples with relatively equally developed textural domains in both perpendicular thin-sections (Fig. 7a). Strong clusters of all mean AMS directions characterise the samples with strongly asymmetrically developed Type I fabrics. Clustering of the measured specimens in a *P–T* plot is typical for all Type I fabrics (Fig. 8a).

Besides measurements of sanidine crystallographic orientation in conjugate textural domains in both K_1K_3 and K_2K_3 thin-sections for Type I fabrics, CPO of groundmass crystals outside the textural domains was also measured in automatic mode (EBSD measurements within 1.2 × 0.6 mm area and 10 μm step-size grid) in the K_1K_3 section of sample 14 to complement the textural description of Type I fabric. The AMS fabric element correlates with both the combined CPO of sanidine textural domains and the groundmass sanidines not belonging to CTDs (Fig. 9). Combined CPO data from all CTDs reveal ring-like distribution of three to four sub-maxima of (010) poles in the stereographic projection. This pattern is similar to that obtained by Jančušková et al. (1992), who showed four sub-maxima in several samples. In addition, the submaxima appear to be orthogonally distributed with respect to the AMS fabric, with two submaxima within the K_1K_3 plane.

The V_1, V_2 and V_3 eigenvector directions of the Lisle's orientation tensor (Lisle, 1989), calculated for triples of poles to (001),(100) and (010) crystallographic planes of sanidines from CTDs, reveals good fit between distribution of poles to (010) directions (V_3 eigenvector) and the K_3 AMS direction (Fig. 9). The V_1 and V_2 directions corresponding to (001) and (100) poles mostly coincide with neither K_1 nor K_2 AMS directions, although in Fig. 9 the V_2 direction appears close to K_1 and V_1 close to K_2.

In contrast to CPO in sanidine textural domains, the poles to (010) planes of groundmass sanidine microphenocrysts outside the CTDs define a polar concentration with K_3 again closely related with V_3 eigenvector, whereas poles to both (100) and (001) planes show elliptical maxima elongated along K_1K_2 plane of AMS ellipsoid and correspond to its K_2 and K_1 directions, respectively.

3.3.4. Type II fabric

In Type II fabric, the sanidine crystals within the textural domains are aligned at high angle to the domain boundary (Fig. 6), and the domain boundaries are sharp and rather irregular. In a plane perpendicular to the fold axis, the angle between alignment

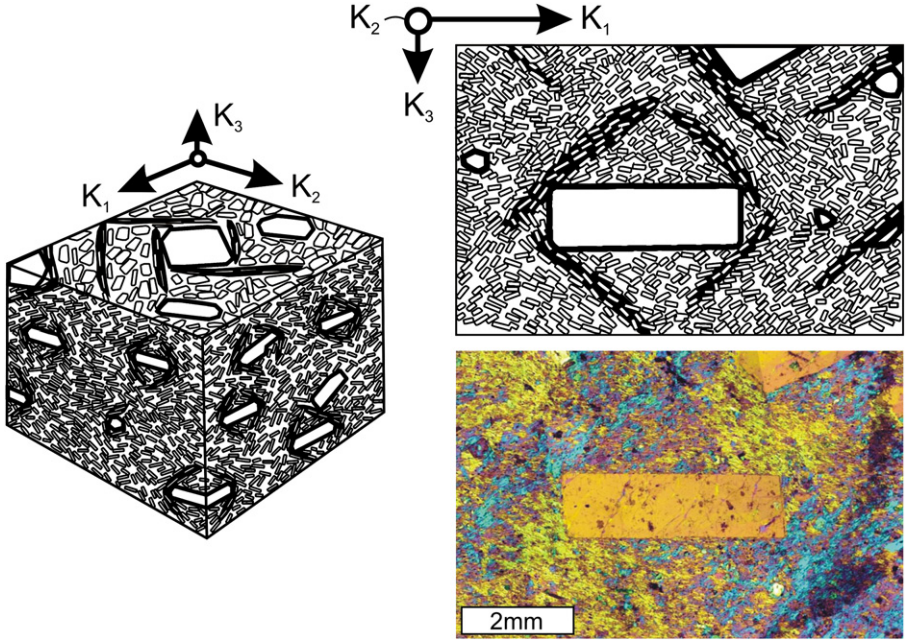

Fig. 5. Microdiagram and map of microsanidine crystal alignment showing conjugate textural domains (CTDs) around phenocrysts in Type I fabrics. CTDs are shown as dark areas in the block diagram and sketch. Micrograph was taken with cross polarised light and gypsum plate. AMS principal axes are shown for reference.

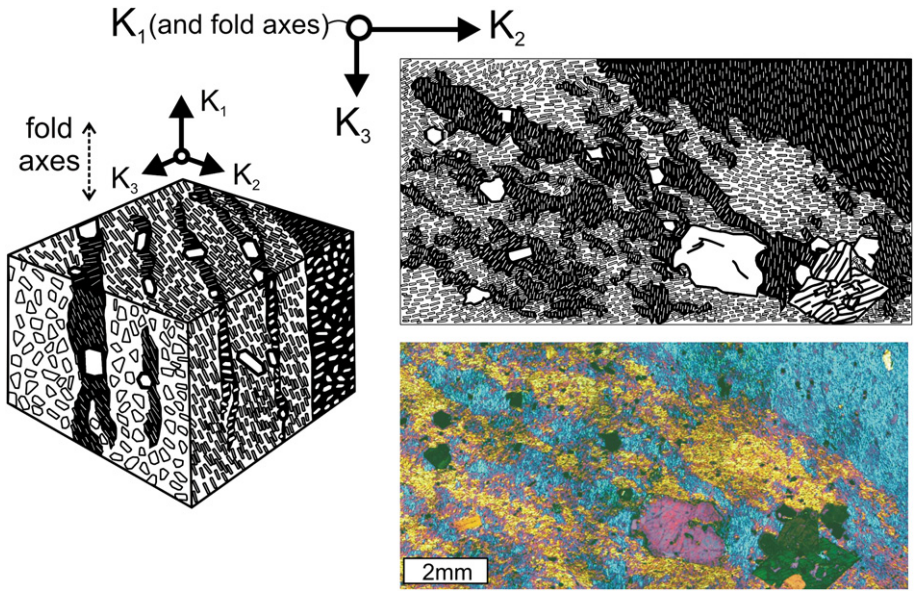

Fig. 6. Microdiagram and map of sanidine crystal alignment showing textural domains in Type II fabric in black. Micrograph taken with cross polarised light and gypsum plate. AMS principal axes and orientation of the fold axes are shown for reference.

trends of crystals in both domains ranges from 45° to 90°. Inspection of the thin-sections cut along the fold axis also revealed that in these sections the textural domain boundaries are parallel to the axial planes (Fig. 6). All samples showing Type II fabric are located in the folded SW part of the body and are characterised by P values between 0.099 and 0.829 (Fig. 4).

Type II fabrics show systematic decrease of one textural domain at the expense of the second domain with increasing chevron-fold amplification (Fig. 10). For example, as the interlimb angle decreases from 70° to 35°, the domain ratio d_1/d_2 decreases from 0.48 to 0.13 for the four samples illustrated in Fig. 10.

Type II fabrics show diffuse clusters of K_1 and K_2 directions and narrow to slightly diffuse clusters of K_3 directions in stereographic projections (Fig. 7b) and discrete clusters of AMS parameter values in P–T plots (Fig. 8b). These geometries are explained by combination of sub-fabrics forming the fold limbs in four measured specimens, which generate smaller values of P and T parameters. The rest of the measured specimens does not show any fabric discontinuity and have P and T values characteristic of Type I samples. Average P and T values also increase with the degree of fold amplification (compare samples 59-A, 60 and 59-B in Fig. 10).

CPO measurements of both textural domains in Type II fabric show two crossed girdles for poles to both (100) and (001) planes, respectively (Fig. 9). The intersection of the girdles is marked by V_1 eigenvector direction of the Lisle's orientation tensor, which is also parallel with the fold axis and K_1 direction of AMS ellipsoid. The K_3 AMS direction coincides with a submaximum of poles to (010) planes corresponding to sanidines from the dominant domain. The V_3 eigenvector direction divides the submaxima of (010) planes, because equal number of crystals was measured from each textural domain.

Table 1
Average AMS parameters from eight measured cubic specimens and results of image analysis for Type I samples.

Sample	AMS parameters		Section	d_1/d_2	Area%		φ
	P	T			d_1	d_2	
18	1.26	0.869	K_1K_3	1.8	0.3	0.2	106
			K_2K_3	1.1	0.2	0.2	105
20	1.249	0.961	K_1K_3	1.9	0.1	0.3	101
			K_2K_3	4.2	0.5	0.1	128
23	1.285	0.797	K_1K_3	1.1	0.2	0.1	–
			K_2K_3	2.4	0.3	0.2	–
83	1.252	0.802	K_1K_3	1.2	0.3	0.2	119
			K_2K_3	2.2	0.4	0.1	102
14	1.256	0.961	K_1K_3	1.5	0.3	0.2	121
			K_2K_3	2.2	0.4	0.1	127
40	1.239	0.945	K_1K_3	1.2	0.2	0.2	103
			K_2K_3	1.3	0.2	0.2	110
38	1.199	0.917	K_1K_3	1.4	0.3	0.2	120
			K_2K_3	1.4	0.3	0.2	112

The relative modal content of textural domains in thin-sections is represented as the ratio d_1/d_2 from two perpendicular thin-sections cut parallel to K_1K_3 and K_2K_3 planes of the magnetic ellipsoid. Note the high values (>1.8) of d_1/d_2 ratios indicating asymmetrical fabric typical for the first four listed samples. "Area%" corresponds to the area fraction of the specific domain with respect to the remaining area of the thin-section. φ indicates the obtuse angle comprised between the conjugate textural domains (from CPO analysis using EBSD).

3.4. Spatial distribution of fabrics

To understand the mechanism of trachyte lava emplacement, the spatial distribution of fabrics throughout the exposed cupola needs to be determined. Samples in the western margin of the

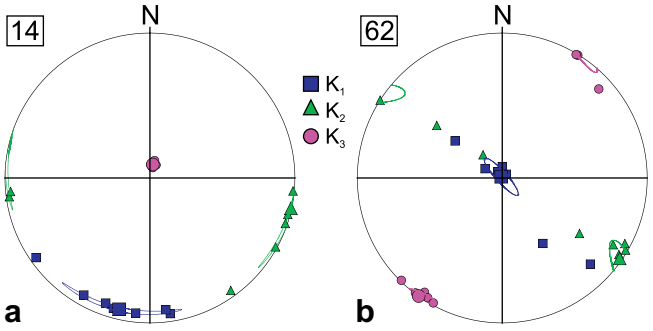

Fig. 7. Stereographic diagrams showing major susceptibility directions (8 specimens measured) of Type I (a) and Type II (b) samples. Equal area, lower-hemisphere projections in geographic coordinates.

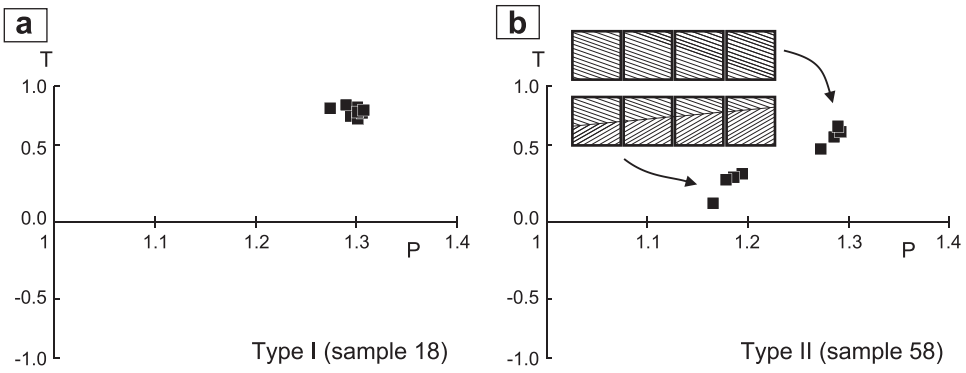

Fig. 8. *P–T* plots of AMS fabric showing distribution of individual cubic specimens in a single sample. Note distribution of specimens in two clusters for Type II fabrics, which reflects presence of discontinuous fabric transition (axial plane of a fold) in four specimens, while the second group attains *P* parameter (AMS fabric intensity) of Type I fabric specimens.

cupola are characterised by Type I fabric with subvertical alignment of large phenocrysts and equally developed CTDs. In all samples from eastern part of the cupola, Type I fabric is marked by asymmetrically developed CTDs. This asymmetry is generally developed in a plane perpendicular to the "F-joints" and parallel to their dip (Fig. 11).

The dominant textural domains (d_1) on the eastern slope dip eastward except for the marginal part, where they dip to the west

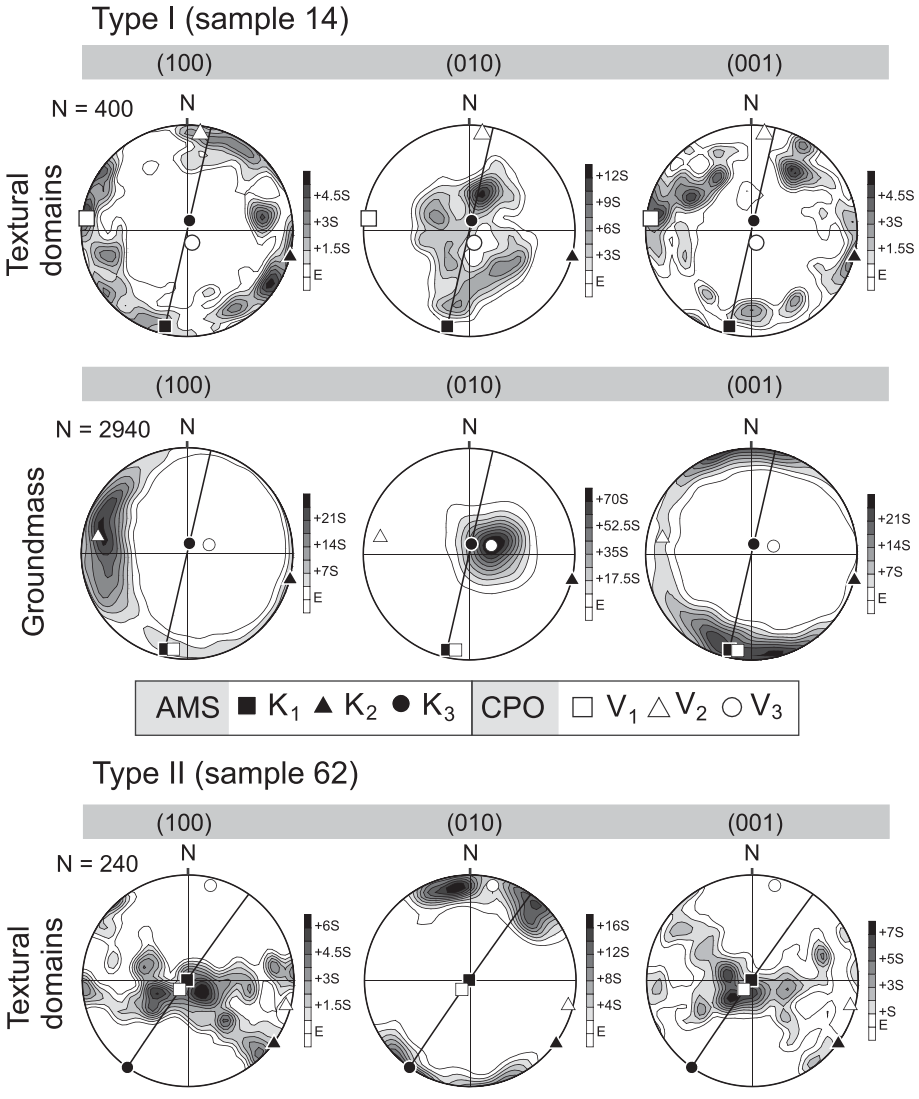

Fig. 9. Combined CPO (crystal preferred orientation) data for Type I and Type II fabrics in equal area, lower-hemisphere stereographic projections for geographic coordinates. Sanidine textural domains for Type I fabrics are represented by combined CPO data from K_1K_3 and K_2K_3 sections (total 400 measurements). "Groundmass" dataset (Type I fabrics) represents CPO of microsanidines obtained by EBSD measurements in automatic mode outside the sanidine textural domains (duplicate measurements were not plotted). Average AMS mean susceptibility directions and K_1K_3 plane (solid black line) are indicated for comparison. The V_1, V_2 and V_3 are eigenvectors of the Lisle's orientation tensor corresponding with poles to (001), (100) and (010) sanidine crystallographic planes.

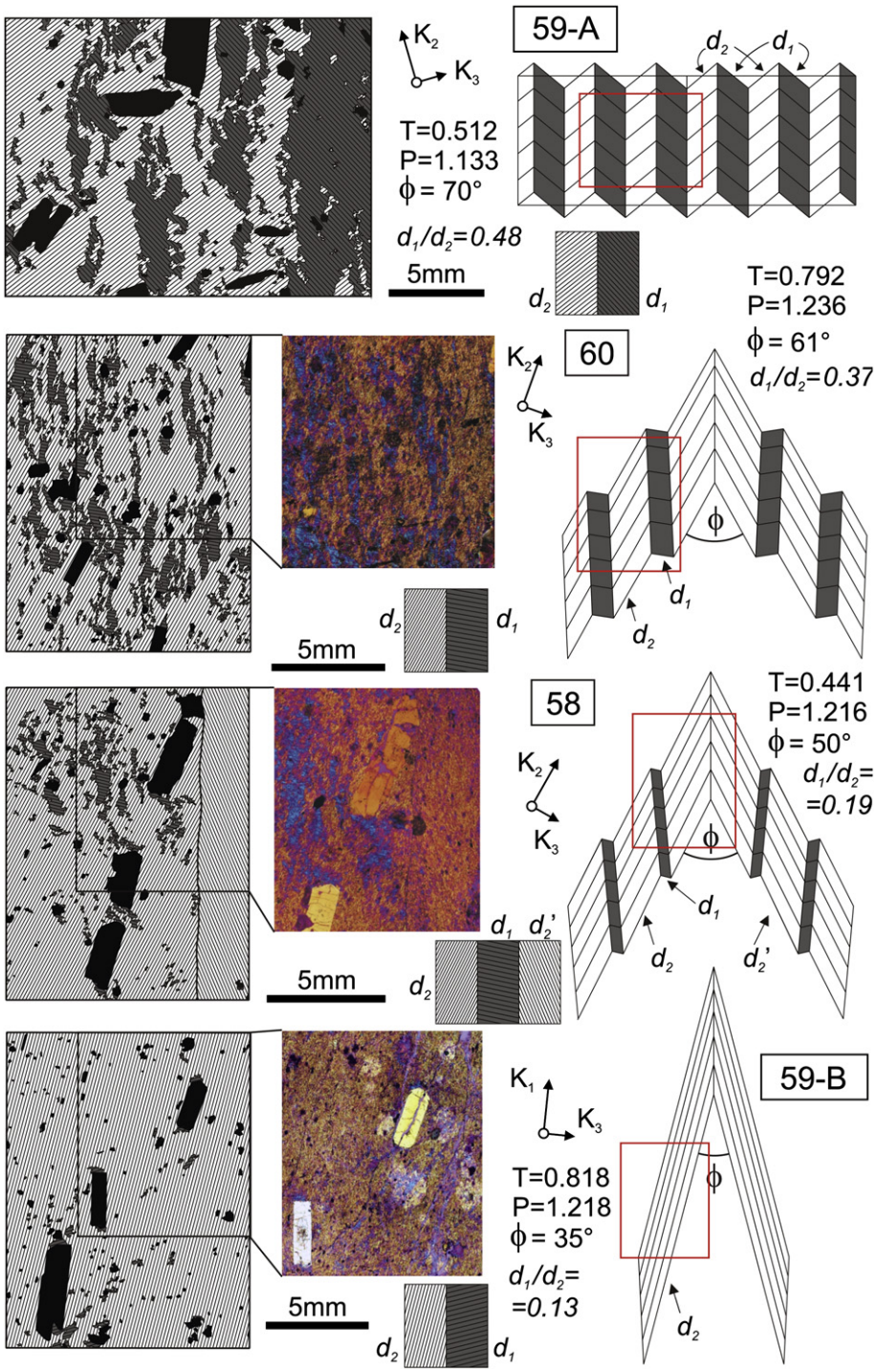

Fig. 10. Traced boundaries of Type II fabric textural domains from fold limbs for increased fold amplitude, indicated by the decreasing inter-limb angle (φ). Alignment of sanidine microcrystals in domains is indicated by hatching. Sample 59-A is from a fold hinge zone. Scale bars refer to traced pictures. Mean susceptibility directions and values of AMS parameters together with domain proportions are indicated. Approximate positions of traced pictures in folds are shown by red rectangles.

(Fig. 11). Close to the central part, the textural domains d_1 are narrow, disjunctive and their length exceeds the thin-section dimensions. Further east these domains become more diffuse and finally fade out to narrow patches on the eastern extremity of the cupola.

The SW part of the body is marked by macroscopic folding and Type II fabrics. Although most of the folds have subvertical axial planes trending NW–SE, in thin-section of sample 58 (corresponding to the northern submaxima of P parameter anomaly, Fig. 4b) the axial fold plane dips at a steep angle to the SW and fold axes are horizontal, trending NW–SE.

4. Discussion

The investigated trachyte represents an example of a solidified dense crystalline mush, without any microscopically observable traces of interstitial quenched melt. The trachyte microstructure

contains textural domains, which suggest that this crystalline mush was actively deforming during or at final stages of trachyte magma emplacement (Smith et al., 1994; Smith, 2000).

Deformation mechanisms and rheology of crystal-rich magmas or metamorphic rocks with small amount of melt are still a matter of debate (Rosenberg, 2001; Závada et al., 2007). Vigneresse et al. (1996) suggested that 75 vol.% of solid particles suspended in a liquid marks the PLT—"particle locking threshold", a critical limit, when the solid–liquid system becomes practically undeformable in magmatic state. Only localisation of deformation into discrete shear zones or formation of S–C like imbrication of magmatic phenocrysts would then accommodate deformation in strongly crystalline magmatic systems close to the PLT (Jančušková et al., 1992; Smith, 1998; Vigneresse and Tikoff, 1999). Imbrication of the phenocrysts into conjugate pairs or single sets of textural domains was identified in several microstructural studies of crystal-rich lavas (Smith et al., 1993a,b, 1994; Smith, 1997). While conjugate domains have been found by both prior and present work, the differences are that in our study, Type I fabric is proximal to phenocrysts, particularly when symmetrically developed and that four zones commonly occur together around each phenocryst (Fig. 6).

We also define another fabric type, which is similar in geometry for microsanidine laths to contractional kink bands typically developed by layer-parallel shortening of a strong mechanical anisotropy shortened parallel to this anisotropy (Price and Cosgrove, 1990). This fabric type is associated with chevron folds in the trachyte.

4.1. Structural interpretation of textural domains

Crystal-alignment textures are useful kinematic indicators of magmatic flow (Ventura et al., 1996; Smith, 1998; Castro et al., 2002). In crystal-rich lavas, conjugate or asymmetric textural domains defined by preferred orientation (CPO) were interpreted to result from coaxial and non-coaxial shear of lava, respectively (Smith, 2002). The origin of these domains was attributed either to: (1) limited late-stage shearing of almost solidified lava (Smith et al., 1993a,b); or (2) reflecting the "shear thickening" rheology of the magma and opening of cavities, because some textural domains contained relatively larger amounts of interstitial melt (Smith, 2000). Both mechanisms can be excluded for our study, because: (1) textural domains are found in all parts of the exposed trachyte cupola, which is also eroded, and are therefore not exclusively from solidifying surficial parts of extrusive bodies (Smith et al., 1993b); and (2) domains enriched in residual melt are absent. Therefore, we consider another deformation mechanism to be responsible for the origin of the textural domains and trachyte magma flow. To interpret the fabrics in trachyte, we rely on analogy with deformation experiments on mica crystals (Tullis, 1976) and theoretical analysis for alternating slip system domains (Cobbold and Gapais, 1986; Gapais and Cobbold, 1987), because appropriate experiments for systems resembling the trachyte magma have not yet been conducted.

4.1.1. Kinematic model of Type I fabric

In the deformation experiments for fine-grained mica aggregates at room temperature, grain interactions impeded grain rotation and the CPO strength remained stable after initial compaction, although the aggregate further deformed (Tullis, 1976). Since all groundmass sanidine crystals in the studied trachyte are lath-like and uncorroded, indicating that they did not change shape during deformation, and evidence for late-stage interstitial melt is absent, we suggest that the process of Type I fabric formation in trachyte lava is analogous to the deformation experiments with fine mica flakes. This analogy is supported by similar CPO patterns of deformed mica aggregates and Type I microsanidine fabric outside the textural domains, both revealing a strong polar maxima of poles to large faces of deformed lath or flake-like crystals. The maximum of poles to basal planes corresponds to the direction of short axis of the finite strain ellipsoid (Tullis, 1976).

We suggest that the Type I microstructure is the result of "quasi-viscous" flow/deformation of trachyte lava facilitated by slip along (010) faces of microsanidine laths. The conjugate CTDs are interpreted as zones of locally greater groundmass distortion by inter-crystalline slip accommodating the presence of large phenocrysts. The microsanidines from the groundmass reveal stronger degree of CPO than that of all the CTDs together, because the crystal-mush flow accommodated by the inter-crystalline slip is more homogeneous away from the phenocrysts. Close spatial relationship between maximum of poles (001) and the AMS lineation suggests that the clusters of poles to (001) measured from the groundmass approximate the local stretching direction of trachyte lava flow. Based on the deformation experiments on micas, where the maximum compressive direction is indicated by the centre of poles to basal planes of mica crystals, shortening during trachyte lava flow is indicated by V_3 eigenvector of the groundmass sanidine crystals (and K_3 mean susceptibility) and also by V_3 direction of the

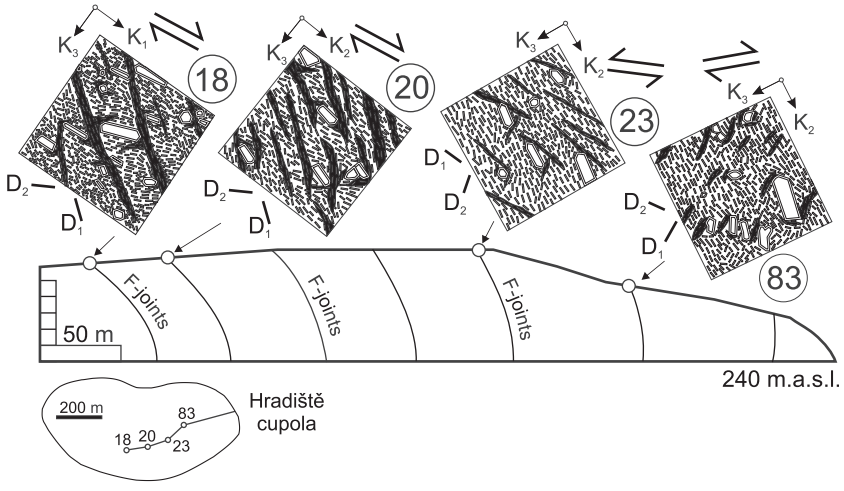

Fig. 11. Profile showing variations in Type I fabrics throughout the eastern part of the cupola. Dominant textural domain (d_1) in Type I fabrics decreases in abundance eastward and changes orientation with respect to alignment of large phenocrysts and F-joints. All sections are subvertical and strike ENE.

CPO from all CTDs. We further assume that the maximum extension direction is indicated by the V_1 direction corresponding to maximum of poles to (001) planes of sanidines in the groundmass, which is parallel with the K_1 mean susceptibility.

4.1.2. Kinematic model of Type II fabric

Similar chevron folds as in the trachyte lava are expected to develop during shortening parallel to the mechanical anisotropy in materials, which are strongly anisotropic (Latham, 1983; Price and Cosgrove, 1990). This anisotropy is defined by parallel alignment of rigid sanidine crystals in the trachyte. We suggest that the initial stage of trachyte lava buckling is preserved in the hinge zones of the folds with the greatest interlimb angle and least amplitude (sample 59-A) showing equally developed Type II fabric domains, with textural domain bands defining small scale chevron folds with wavelength of 5 mm (Fig. 10). Fold amplification for much larger wavelength than 5 mm induces simple shear with opposite vorticities in fold limbs (samples 60 and 58), which results in rearrangement of initially regularly developed textural domains as in the "fibre-slip" model of Cobbold and Gapais (1986). According to this model, deformation of an aggregate consisting of parallel band-like domains formed by undeformable fibres is accommodated by simultaneous slip along individual fibres (sanidine lath-like crystals) and the slip along these fibres is again characterised by opposite vorticity in each domain (Mode I). One set of domains can be consumed by the second set by simple migration of the boundaries between them (Fig. 12, Mode II), as fibres rotate past the migrating boundary and are incorporated into the adjacent domain.

Combination of both modes of fibre-slip model can accommodate large amounts of finite strain, if fibres of one domain are oriented at low angle to the direction of shear. Furthermore, Mode III motion of fibre-slip model can explain rotation of domain boundaries by motion of material through the domain boundaries (Cobbold and Gapais, 1986). We suggest the Mode II motion to be responsible for accommodation of simple shear in chevron fold limbs of the trachyte lava by modification of the initial geometry represented by equally developed domains in chevron folds such as in sample 59-A. Minor contribution of Mode III motion can explain small angular misfit between trends of textural boundaries and chevron fold planes (Fig. 12d,e).

Extreme angularity, dip symmetry and straightness of limbs manifested by trachyte folds reflect the relative ease of slip and relative difficulty of stretch along the alignment direction of microsanidine laths (Cobbold and Gapais, 1986). The folds are interpreted to have formed by shortening parallel to the initial mechanical anisotropy and we assume that the shortening direction is approximated by the normal to the axial plane of folds, because most of the observed folds are relatively symmetrical. The extension direction is perpendicular to fold axis and within the axial plane, and corresponds to K_1 mean susceptibility for the most amplified fold (sample 59-B). The shortening direction for Type II fabrics, where fold axial planes are not preserved, remains speculative. An estimate though is given by a normal to the boundaries between Type II textural domains, which is subparallel to the axial plane (Fig. 12).

4.2. The emplacement level and the strain field distribution throughout the cupola

The orientation (strike and dip direction) of sanidine fabrics and F-joints define overall an onion-like structure of the cupola. The fabrics locally overturn on the margins of the body, which means that the exposed trachyte cupola is probably topping an upward widening stem above the thick and competent basanite lava sequence. We therefore suggest that the body represents a remnant of an extrusive dome. The high angle between the fabrics and the topography of the exposed body suggests it was deeply eroded.

4.3. Kinematics of lava flow in the trachyte dome

Analogue experiments using silicone putties or pseudoplastic slurries and numerical simulations (Buisson and Merle, 2004; Závada et al., 2008) revealed that the poles to maximum shortening direction, approximated by K_3 directions for Type I fabrics, direct towards the vent zone feeding the lava dome with new material. The extension directions approximated by directions of magnetic lineation K_1 for the trachyte body are simultaneously mostly subhorizontal and parallel with the margin of the body due to circumferential stretching, which intensifies with distance from the central part of lava dome extrusions (Merle, 1998; Buisson and Merle, 2002; Buisson and Merle, 2004; Závada et al., 2008). Interpretation of the CPO and AMS fabric data for the trachyte body together with fold geometries suggests that the maximum shortening directions converge on the cupola centre (Fig. 13).

The sequence of samples with asymmetric Type I fabrics in eastern part of the cupola (20, 23, 83) probably reveal non-coaxial lava flow due to gradients in lateral flow velocity in extrusive lava domes (Buisson and Merle, 2002, 2004). However, the interpretation of their shear sense in a plane perpendicular to the maximum stretching direction is speculative (Fig. 11). The western margin, marked by steep fabric and subhorizontal lineation, is also interpreted to record circumferential and coaxial stretching of lava.

4.4. The mechanism of folding and fabric transitions

We propose an emplacement model that could result in the observed fabric zonality, which is based on AMS analogue modelling of fabric development in complex lava domes (Závada et al., 2008). According to this model, lobes of lava emerge and are rotated and translated sideways due to emplacement of younger lobes. In this context, three mechanisms possibly explain the origin of chevron folds with steep axes in the trachyte body: (1) inflation of the lastly emplaced lava portion, which transposed the fabrics in earlier emplaced lava units; (2) collapse of vertical fabrics from the conduit (Smith and Houston, 1995) preserved in the interior of a rotated lobe of lava (Fig. 14); or (3) the folds are "curtain folds" typically developed in vertical channels of salt diapirs (Talbot and Jackson, 1987). According to the analogue modelling results (Závada et al., 2008), it is most probable that the folds formed due to the second mechanism, which reflects the divergent flow in lava lobes above the vent. The remnants of folds could be preserved within a lava lobe, which was rotated and transported "en-masse" towards the dome margin by a newer lava portion (Závada et al., 2008). It is not probable that the folds are "curtain folds", developed by folding of the sanidine fabric in the vertical conduit, because the anisotropy defined by alignment of sanidine laths has short strain memory in contrast to passive markers of coloured salt layers in the salt diapir (Talbot and Jackson, 1987).

The outlined scenario implies that the Type II fabric, associated with chevron folds, is older than Type I fabrics. Where Type II fabric domains disappear by the fibre-slip mechanism (Figs. 10 and 12) due to continuous layer-perpendicular shortening, replacing layer-parallel shortening (Ramsay, 1967), Type I fabric textural domains should start to form, because the lava is continuously vertically flattened and radially stretched above the vent zone (Fig. 14) (Závada et al., 2008). The transitional stage between Type II and Type I fabric is probably represented by sample 59-B (Fig. 10), corresponding to the most amplified fold. This interpretation means that the strong sanidine crystal alignment in the

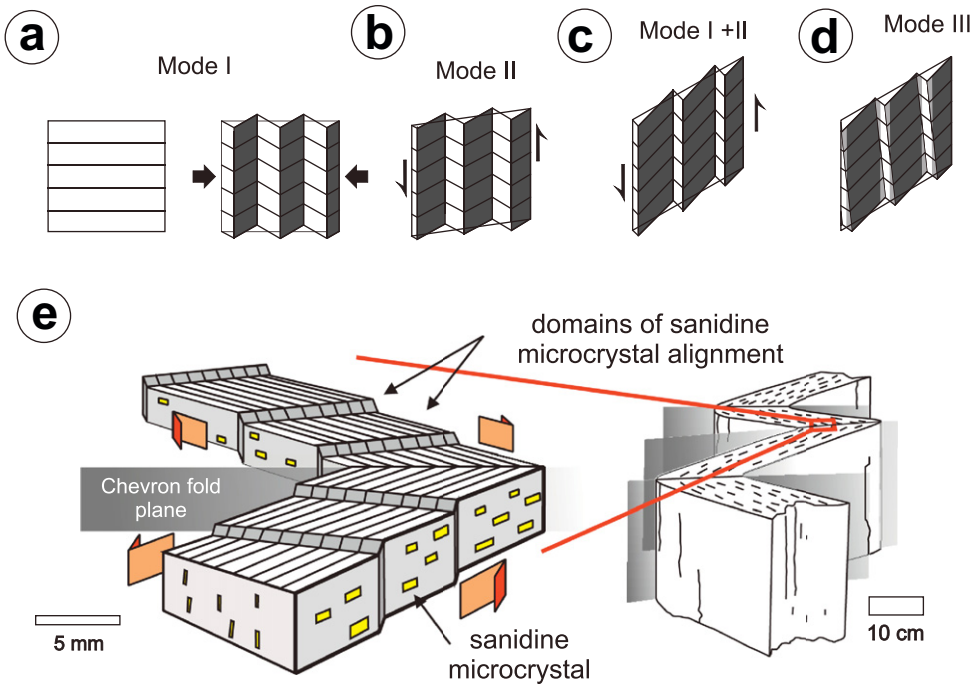

Fig. 12. Modes of motion in "fibre-slip" model (Cobbold and Gapais, 1986) and evolution of the domains in Type II fabric with progressive deformation. Deformation of an aggregate consisting of band-like domains formed by parallel alignment of fibres (e.g. sanidine lath shaped crystals) is facilitated by: (a) Mode I—slip of fibres along each other within each domain; (b) Mode II—movement of boundaries between the domains; (c) combination of Mode I and Mode II mechanisms; (d) Mode III—rotation of domain boundaries due to material migrating across the domain boundary (light grey area indicates the material that passed through the domain boundary). (e) Schematic block diagram depicting the kinematic interpretation of Type II fabrics in three dimensions.

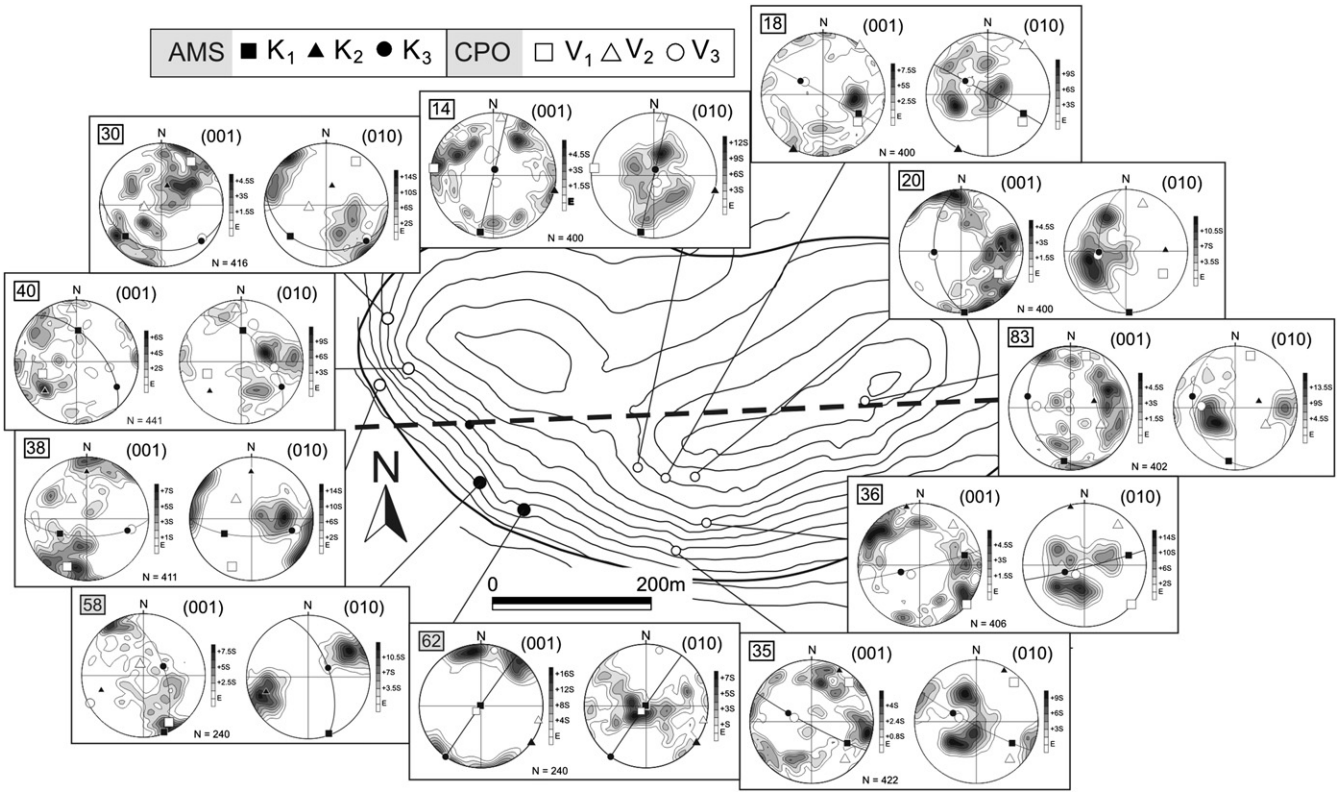

Fig. 13. Diagram showing distribution of poles to (001) and (010) of sanidines in CTDs with eigenvectors for Lisle's orientation tensor and AMS mean susceptibility directions throughout the studied cupola. Lower-hemisphere equal area projections in geographical coordinates. Contours indicate multiples of uniform distribution. Samples 58 and 62 in SW part of body have Type II fabrics, whereas other samples have Type I fabrics. Thick dashed line indicates the profile section in Fig. 14.

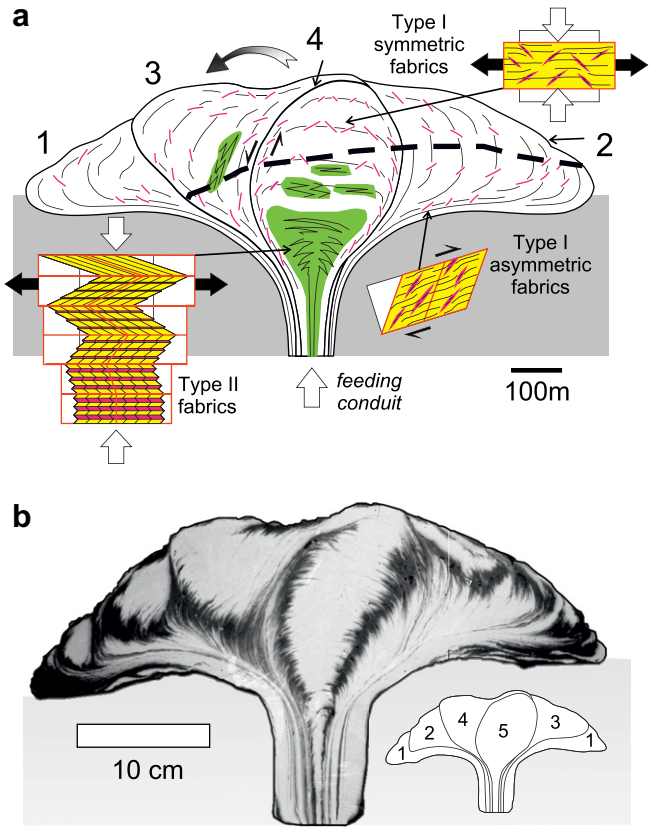

Fig. 14. (a) Interpretative cross-section through the trachyte cupola showing the internal structure of the trachyte body resulting from successive emplacement of individual lava lobes (E–W oriented section, today's exposure is indicated by thick dashed line). Each new lava lobe rises along a shear zone cross-cutting the earlier emplaced lobe. Older lava units are being rotated and transported sideways as new lava lobes form and rise to the summit of a lava dome. Asymmetric chevron folds forming the Type II fabrics originate in the bottom interior of each rising lobe due to collapse of vertical fabrics from the conduit. Domains of folded fabrics that can be preserved in rotated lobes are indicated in green. (b) Cross-section through an analogue model of lava extrusion created by plaster of Paris (from Závada et al., 2008). Interpretation of outlines for successively emplaced individual plaster lobes is indicated.

groundmass of Type I fabrics is partly inherited from the alignment of the d_2 domain of Type II fabrics in highly amplified folds and intensified by further flattening of lava due to divergent flow.

The eastern part of the cupola would represent the earlier emplaced lava portions, which gravitated from flanks of the dome and underwent circumferential stretching as a result of divergent flow (Merle, 1998; Buisson and Merle, 2002, 2004; Závada et al., 2008). The western part of the cupola in the presented scenario corresponds to the rotated lobe with locally preserved folded domains (Fig. 14).

5. Conclusions

Combined AMS and detailed microstructural analysis including image analysis of textural domains and CPO of sanidine laths provides a basis for description and interpretation of fabrics within trachyte bodies. In the Hradiště dome, two fabric types, Type I and Type II, are associated with shortening of trachyte lava perpendicular and parallel, respectively, to the mechanical anisotropy from the preferred alignment of sanidine laths. Variations of Type I and Type II fabrics can possibly represent a continuous sequence of trachyte fabric development during emplacement of the dome. This sequence would be as follows: collapse of vertical fabric above the conduit (development of Type II fabrics), further flattening in dome's apical parts (transition from Type II to Type I) and circumferential stretching together with non-coaxial strain component in plane normal to the stretching producing asymmetric Type I fabric on the flanks and base of the domes. Irregularities in spatial distribution of fabrics would arise from emplacement of "lobes" of lava that can partly conserve fabrics in their interior.

Acknowledgements

This work was funded from the grant of the Czech Science Foundation (GAČR), No. 205/03/0204 and the "Junior grant" of the Grant agency of the Czech Academy of Sciences (GAAV), No. B301110703. We are grateful to William M. Dunne for editing the manuscript. We thank Manuel Díaz Azpiroz and an anonymous reviewer for their careful reviews that helped to improve the first draft.

References

Arbaret, L., Diot, H., Launeau, P., 1993. Le Suc phonolitique du Petit Gerbier (Velay, Massif Central); fabriques magnétique et magmatique. Comptes Rendus de l'Académie des Sciences, Série 2, Mécanique, Physique, Chimie, Sciences de l'Univers, Sciences de la Terre 316 (11), 1603–1610.
Buisson, C., Merle, O., 2002. Experiments on internal strain in lava dome cross sections. Bulletin of Volcanology 64 (6), 363–371.
Buisson, C., Merle, O., 2004. Numerical simulation of strain within lava domes. Journal of Structural Geology 26 (5), 847–853.
Cañón Tapia, E., Castro, J., 2004. AMS measurements on obsidian from the Inyo Domes, CA: a comparison of magnetic and mineral preferred orientation fabrics. Journal of Volcanology and Geothermal Research 134 (3), 169–182.
Cajz, V., Vokurka, K., Balogh, K., Lang, M., Ulrych, J., 1999. The české Středohoří Mts.: volcanostratigraphy and geochemistry. Geolines 9, 21–28.
Castro, J., Manga, M., Cashman, K., 2002. Dynamics of obsidian flows inferred from microstructures: insights from microlite preferred orientations. Earth and Planetary Science Letters 199, 211–226.
Clark, P., Evans, F., 1954. Distance to nearest neighbor as a measure of spatial relationships in populations. Ecology 35, 445–453.
Cloos, H., 1922. Tektonik und Magma. Untersuchungen zur Geologie der Tiefen. Abhandlungen der Preussischen Geologischen Landesanstalt 1 (89).
Cloos, H., Cloos, E., 1927. Die Quellkuppe des Drachenfels am Rhein. ihre Tektonik und Bildungsweise. Zeitschrift für Vulkanologie XI, 33–40.
Cobbold, P.R., Gapais, D., 1986. Slip-system domains. 1. Plane-strain kinematics of arrays of coherent bands with twinned fibre orientations. Tectonophysics 131, 113–132.
Dewey, J.F., 1965. Nature and origin of kink-bands. Tectonophysics 1 (6), 459–494.
Fink, J.H., 1983. Structure and emplacement of a rhyolitic obsidian flow: Little Glass Mountain, Medicine Lake Highland, northern California. Geological Society of America Bulletin 94, 362–380.
Gapais, D., Cobbold, P.R., 1987. Slip system domains. 2. Kinematic aspects of fabric development in polycrystalline aggregates. Tectonophysics 138, 289–309.
Harvey, P., Ferguson, C., 1981. Directional properties of polygons and their application to finite strain estimation. Tectonophysics 74, 33–42.
Herrero-Bervera, E., Walker, G.P.L., Cañón Tapia, E., Garcia, M.O., 2001. Magnetic fabric and inferred flow direction of dikes, conesheets and sill swarms, Isle of Skye, Scotland. Journal of Volcanology and Geothermal Research 106 (3–4), 195–210.
Hrouda, F., Jelínek, V., Hrušková, L., 1990. A package of programs for statistical evaluation of magnetic data using IBM-PC computers. AGU 1990 fall meeting. Eos, Transactions, American Geophysical Union 71 (43), 1289.
Hrouda, F., Chlupáčová, M., Schulmann, K., Šmíd, J., Závada, P., 2005. On the effect of lava viscosity on the magnetic fabric intensity in alkaline volcanic rocks. Castle Meeting. Studia Geophysica et Geodetica 49 (2), 191–212.
Hrubcová, P., Sroda, P., Špičák, A., Guterch, A., Grad, M., Keller, G.R., Brueckl, E., Thybo, H., 2005. Crustal and uppermost mantle structure of the Bohemian Massif based on CELEBRATION 2000 data. Journal of Geophysical Research-Solid Earth 110 (B11), Art. No. B11305.
Jančušková, Z., Schulmann, K., Melka, R., 1992. Relation entre fabrique de la sanidine et mise en place des magmas trachytiques (exemple de massif de Hradiste; Boheme du Nord). Geodinamica Acta 5 (4), 235–244.
Jelínek, V., 1978. Statistical processing of anisotropy of magnetic susceptibility measured on groups of specimens. Studia Geophysica et Geodaetica 22, 50–62.
Jelínek, V., 1981. Characterization of magnetic fabric of rocks. Tectonophysics 79, 63–67.

Jelínek, V., Pokorný, J., Richter, A.K., 1997. Some new concepts in technology of transformer bridges for measuring susceptibility anisotropy of rocks. Physics and Chemistry of the Earth 22 (1–2), 179–181.
Kidan, T.W., Cosgrove, J.W., 1996. The deformation of multilayers by layer-normal compression; an experimental investigation. Journal of Structural Geology 18 (4), 461–474.
Kolofíková, O., 1976. Geologická interpretace měření magnetických vlastností čediču na příkladu lávového proudu Chřibského lesa vulkánu Velkého Roudného (Nízký Jeseník), (in czech), Translated title: Geological interpretation of magnetic properties measurements of basalts on example of Chřibský les lava flows of Velký Roudný volcano (Nízký Jeseník mountains). Časopis pro Mineralogii a Geologii 21 (4), 387–396.
Kopecký, L., 1978. Neoidic taphrogenic evolution and young alkaline volcanism of the Bohemian Massif. Sborník Geologických Věd: Geologie (Journal of Geological Sciences: Geology), 91–107.
Latham, J., 1983. The influence of mechanical anisotropy on the development of geological structures. Ph.D. thesis, University of London.
Lexa, O., Štípská, P., Schulmann, K., Baratoux, L., Kröner, A., 2005. Contrasting textural record of two distinct metamorphic events of similar *P–T* conditions and different durations. Journal Of Metamorphic Geology 23 (8), 649–666.
Lisle, R., 1989. The statistical analysis of orthogonal orientation data. Journal of Geology 97 (3), 360–364.
Macák, F., 1963. Basic geological map, scale 1:50000, sheet M-33-52-B, Teplice. Report. Geofond Prague P 15 674.
Maeno, F., Taniguchi, H., 2006. Silicic lava dome growth in the 1934–1935 Showa Iwo-jima eruption, Kikai caldera, south of Kyushu, Japan. Bulletin of Volcanology 68 (7–8), 673–688.
Melnik, O., Sparks, R.S.J., 1999. Nonlinear dynamics of lava dome extrusion. Nature 402 (6757), 37–41.
Merle, O., 1998. Internal strain within lava flows from analogue modelling. Journal of Volcanology and Geothermal Research 81 (3–4), 189–206.
Nagata, T., 1961. Rock Magnetism. Maruzen, Tokyo, 350 pp.
Nakada, S., Yasuyuki, M., Sato, H., Oshima, O., Fujinawa, A., 1995. Endogenous growth of dacite dome at Unzen volcano (Japan), 1993-1994. Geology 23 (2), 157–160.
Plomerová, J., Achauer, U., Babuška, V., Granet, M., Boušková, A., Brauer, K., Brož, M., Brunner, M., Fischer, T., Funke, S., Geibler, W., Heuer, B., Horálek, J., Jedlička, P., Kampf, H., Kind, R., Klinge, K., Kolář, P., Korn, M., Lindemann, M., Málek, J., Malischewski, P., Nehybka, V., Novotný, O., Plenefisch, T., Plomerová, J., Robler, D., Ružek, B., Stammler, K., Vavryčuk, V., Vecsey, L., Wendt, S., Zedník, J., Bohema Working Group, I., 2003. BOHEMA 2001–2003; passive seismic experiment to study lithosphere-asthenosphere system in the western part of the Bohemian Massif. Studia Geophysica et Geodetica 47 (3), 691–701.
Pokorný, J., Suza, P., Hrouda, F., 2004. Anisotropy of magnetic susceptibility of rocks measured in variable weak magnetic fields using the KLY-4S Kappabridge. Geological Society Special Publication 238, 69–76.
Price, N., Cosgrove, J.W., 1990. Analysis of Geological Structures. Cambridge University Press, Cambridge, UK, 502 pp.
Ramsay, J.G., 1967. Folding and Fracturing of Rocks. McGraw-Hill, New York, 567 pp.
Raposo, M., Ernesto, M., 1995. Anisotropy of magnetic susceptibility in the Ponta Grossa dyke swarm (Brazil) and its relationship with magma flow direction. Physics of the Earth and Planetary Interiors 87 (3–4), 183–196.
Rosenberg, C.L., 2001. Deformation of partially molten granite: a review and comparison of experimental and natural case studies. International Journal of Earth Sciences 90 (1), 60–76.
Scambos, T., Smyth, J., McCormick, T., 1987. Crystal structure refinement of a natural high sanidine of upper mantle origin. American Mineralogist 72 (9–10), 973–978.
Schmidt, N.H., Olensen, N., 1989. Computer-aided determination of crystal-lattice orientation from electron-channelling patterns in the SEM. Canadian Mineralogist 28, 15–22.
Smith, J., Houston, E., 1995. Folds produced by gravity-spreading of a banded rhyolite lava flow. Journal of Volcanology and Geothermal Research 63, 89–94.
Smith, J.V., 1997. Shear thickening dilatancy in crystal-rich flows. Journal of Volcanology and Geothermal Research 79 (1–2), 1–8.
Smith, J.V., 1998. Interpretation of domainal groundmass textures in basalt lavas of the southern Lamington Volcanics, eastern Australia. Journal of Geophysical Research, Solid Earth 103 (B11), 27383–27391.
Smith, J.V., 2000. Textural evidence for dilatant (shear thickening) rheology of magma at high crystal concentrations. Journal of Volcanology and Geothermal Research 99 (1–4), 1–7.
Smith, J.V., 2002. Structural analysis of flow-related textures in lavas. Earth-Science Reviews 57 (3–4), 279–297.
Smith, J.V., Miyake, Y., Yamauchi, S., 1993a. Flow direction and groundmass shear zones in dykes, Shimane Peninsula, Japan. Geological Magazine 130 (1), 117–120.
Smith, J.V., Yamauchi, S., Miyake, Y., 1993b. Microshear zones in a Miocene submarine dacite dome of southwest Japan. Bulletin of Volcanology 55 (6), 438–442.
Smith, J.V., Yamauchi, S., Miyake, Y., 1994. Coaxial progressive deformation textures in extrusive and shallow intrusive rocks, Southwest Japan. Journal of Structural Geology 16 (3), 315–322.
Sparks, R.S.J., Murphy, M.D., Lejeune, A.M., Watts, R.B., Barclay, J., Young, S.R., 2000. Control on the emplacement of the andesite lava dome of the Soufrière Hills Volcano, Montserrat by degassing-induced crystallization. Terra Nova 12, 14–20.
Špičák, A., Horálek, J., 2001. Possible role of fluids in the process of earthquake swarm generation in the West Bohemia/Vogtland seismoactive region. Tectonophysics 336 (1–4), 151–161.
Talbot, C.J., Jackson, M.P.A., 1987. Internal kinematics of salt diapirs. AAPG Bulletin, American Association of Petroleum Geologists 71 (9), 1068–1093.
Tarling, D., Hrouda, F., 1993. The Magnetic Anisotropy of Rocks. Chapman & Hall, London. 217.
Tullis, T.E., 1976. Experiments on origin of slaty cleavage and schistosity. Geological Society Of America Bulletin 87 (5), 745–753.
Uličný, D., 2001. Depositional systems and sequence stratigraphy of coarse-grained deltas in a shallow-marine, strike-slip setting; the Bohemian Cretaceous Basin, Czech Republic. Sedimentology 48 (3), 599–628.
Ulrych, J., Novák, J., Langrová, A., Melka, K., Cajz, V., Adamovič, J., Pertlik, F., Wiesner, T., Žid, L., Radoň, M., 2000. Tertiary phonolite laccolith of Mariánská hora hill, N. Bohemia: geological, petrological and mineralogical characteristics. Acta Montana IRSM AS CR 15 (116), 5–44.
Varet, J., 1971. Structure et mise en place des massifs phonolitique du Cantal (Auvergne, France). Geologische Rundschau 60 (3), 948–968.
Ventura, G., DeRosa, R., Colletta, E., Mazzuoli, R., 1996. Deformation patterns in a high-viscosity lava flow inferred from the crystal preferred orientation and imbrication structures: An example from Salina (Aeolian Islands, southern Tyrrhenian Sea, Italy). Bulletin of Volcanology 57 (7), 555–562.
Vigneresse, J.L., Tikoff, B., 1999. Strain partitioning during partial melting and crystallizing felsic magmas. Tectonophysics 312 (2–4), 117–132.
Vigneresse, J.L., Barbey, P., Cuney, M., 1996. Rheological transitions during partial melting and crystallization with application to felsic magma segregation and transfer. Journal of Petrology 37 (6), 1579–1600.
Závada, P., Schulmann, K., Konopásek, J., Ulrich, S., Lexa, O., 2007. Extreme ductility of feldspar aggregates—Melt-enhanced grain boundary sliding and creep failure: Rheological implications for felsic lower crust. Journal of Geophysical Research, Solid Earth 112, B10210. doi:10.1029/2006JB004820.
Závada, P., Kratinová, Z., Kusbach, V., Schulmann, K., 2008. Internal fabric development in complex lava domes. Tectonophysics, DOI: 10.1016/j.tecto.2008.07.005.